Measurements of the vector analyzing power iT_{11} in the $\pi\vec{d}$ elastic scattering reaction between 117 and 325 MeV

G. R. Smith, E. L. Mathie, E. T. Boschitz, and C. R. Ottermann
Kernforschungszentrum Karlsruhe, Institut für Kernphysik and Institut für Experimentelle Kernphysik der Universität Karlsruhe, D-7500 Karlsruhe, Federal Republic of Germany

S. Mango, J. A. Konter, and M. Daum
Schweizerisches Institut für Nuklearforschung, CH-5234 Villigen, Switzerland

M. Meyer, R. Olszewski, and F. Vogler
Physikalisches Institut, Universität Erlangen-Nürnberg, D-8520 Erlangen, Federal Republic of Germany
(Received 7 February 1984)

The vector analyzing power iT_{11} has been measured for the $\pi\vec{d}$ elastic scattering reaction at 12 incident pion energies between 117 and 325 MeV, using a vector polarized deuteron target. The results cover an average of 14 angles per incident pion energy. A detailed comparison with existing Faddeev calculations is made. The effect of including dibaryon resonances with one of these predictions is investigated.

I. INTRODUCTION

Until recently, the possibility of observing effects related to the quark structure of nuclei was considered remote. Theoretical attempts at addressing this interesting topic have appeared in the literature in recent years in the form of bag model calculations, in which the nucleons are represented by bags of quarks confined by an *ad hoc* pressure. Beyond the description of hadronic ground states (nucleons and mesons), new states of matter composed of combinations of quarks other than qqq or $q\bar{q}$ were predicted. In particular, systems of six quarks with baryon number 2 were postulated (dibaryons), consisting of (hidden) colored subclusters of quarks separated by an angular momentum barrier.[1] The subsequent experimental observation of resonances in the nucleon-nucleon channel close to the predicted masses of some of these states fueled this speculation considerably.[2] More recently, dibaryons have been offered as a possible explanation for the anomalous ratio of structure functions observed in the deep-inelastic scattering of electrons and muons from iron and deuterium nuclei.[3]

In light of the fact that the resonant NN scattering amplitudes have large inelasticities, it is expected that there would be a considerable coupling to the πNN channels. The advantage offered by the πd channel is the availability of a relatively well-understood theoretical treatment in the form of fully relativistic three body Faddeev equations. The dibaryon signals are then expected to appear as deviations from these predictions. Assessing the significance of these deviations is, however, complicated by the fact that refinements in the conventional dynamics (such as N-Δ interactions, Δ-Δ interactions, or heavy meson exchange) may eventually take place. Some measurements of the differential cross section have recently been undertaken in the πd channel in the hopes of uncovering these resonances.[4–6] However, as dibaryon signals are expected to be small, if they exist at all, attention has focused on spin observables which may reveal the effects of small amplitudes from their interference with the larger ones which dominate the differential cross section. The first reported measurements of the vector analyzing power iT_{11} in πd elastic scattering seemed to provide evidence for the existence of at least one resonance,[7] although the quantity of the data was sparse, and the quality poor. Further measurements utilizing the same technique, but including a recoil deuteron telescope, extended the data set to three further energies, but again the few angles available for each energy made a systematic analysis difficult.[8]

In this work we report the results of a comprehensive set of measurements designed to accurately map out the behavior of the vector analyzing power iT_{11} in πd elastic scattering over a wide range of angles and bombarding energies. The results cover an average of 14 angles per energy, for 12 incident energies between 117 and 325 MeV, and take advantage of two different experimental techniques designed to improve the quantity and quality of the data. We then compare this body of data with the existing theoretical calculations and discuss the relevance to the dibaryon problem.

II. EXPERIMENTAL PROCEDURE

A. Overview

In principle there exist two methods to measure polarization observables in the πd elastic scattering reaction. One technique employs a polarimeter to measure the po-

larization of the recoil deuteron in a second scattering. This technique suffers from several drawbacks. In particular, the low rates associated with a double scattering experiment can make it difficult to obtain sufficient statistics in a reasonable time. Furthermore, the technique relies on the availability of recoil deuterons, many of which do not escape the target at low bombarding energies or at small pion scattering angles. The recoil deuterons which are available must often be degraded in order to match their momenta to known analyzing powers in the polarimeter. This method has been applied, however, to measurements of the tensor polarization t_{20} in large angle πd elastic scattering,[9,10] as well as for measurements of the vector polarization iT_{11} in the pp$\rightarrow\pi$d reaction.[11]

A second approach utilizes a polarized deuteron target in a single scattering experiment. The drawback of this approach is the presence of contaminant nuclei in the target material whose presence is required in order to achieve polarization of the deuterons. These constituents of the target (typically carbon, oxygen, helium, and brass) give rise to background events which must be separated from the πd elastic events of interest. Furthermore, polarized targets employ high magnetic fields which affect particle trajectories as well as the performance of detectors in the vicinity. The background problems can be solved by means of a pion beam line with a sufficiently well focused beam at the target location, and a detection system with sufficient resolution to distinguish πd elastic scattering events from other reactions originating from the background nuclei. The SUSI beam line and spectrometer at SIN is such a facility.[12] This facility is, however, limited by the 15 msr spectrometer solid angle. A more efficient method of collecting data is the measurement of the time of flight (TOF) difference between elastically scattered pions and their coincident recoil deuterons using several pairs of large solid angle detectors. This method is essentially limited to the backward hemisphere, where recoil deuterons have enough kinetic energy to escape the target. The data presented here have been obtained using a polarized deuteron target with both the SUSI and the TOF detection systems (in separate experiments) in order to increase both the efficiency and the angular range of the measurements. The details of these techniques will be discussed in the following.

In this experiment the vector analyzing power iT_{11} is determined from measurements of the differential cross sections of the πd elastic scattering reaction for measured values of the target vector polarization. In terms of the three magnetic substates of the deuteron spin system the vector polarization of the target can be expressed as

$$P=\frac{n^+-n^-}{n^++n^-+n^0}\ . \tag{1}$$

The tensor polarization of the target is defined by

$$P_{zz}=T=\frac{n^++n^--2n^0}{n^++n^-+n^0}\ . \tag{2}$$

The normalization is such that $n^++n^-+n^0=1$, where n^+, n^-, and n^0 denote the populations of the magnetic substates of the deuteron, $m=\pm1$, 0. Ignoring contributions from the deuteron quadrupole moment, the tensor polarization can be related to the vector polarization by the expression

$$T=\sqrt{2}\tilde{t}_{20}=2-\sqrt{4-3P^2}\ . \tag{3}$$

In preceding publications,[7,8,13] the magnitude of the target vector polarization was normalized to an upper bound of $\frac{2}{3}$, as is sometimes done with polarized deuteron beams which can produce pure vector polarization. For a vector polarized deuteron target, however, no such constraint on the tensor polarization is imposed. In fact, the vector polarization in a polarized deuteron target can in principle reach values of ±1, with a corresponding tensor polarization given by Eq. (3). Consequently, the values of iT_{11} published previously are in error by this amount $\frac{2}{3}$ and will be presented here correctly normalized, for the sake of clarity.

The expression for the polarized differential cross section is given according to the Madison convention[14] as

$$\sigma^{\pm}(\theta)=\sigma^0(\theta)[1\pm\sqrt{2}\tilde{t}_{10}\langle iT_{11}\rangle-\tfrac{1}{2}\tilde{t}_{20}\langle T_{20}\rangle -\sqrt{3/2}\tilde{t}_{20}\langle T_{22}\rangle]\ , \tag{4}$$

where $\tilde{t}_{10}$ and $\tilde{t}_{20}$ are the vector and tensor target polarizations in spherical coordinates along an axis perpendicular to the scattering plane (parallel to the magnetic field of the target). The superscript (+) indicates the direction of $\vec{k}\times\vec{k}'$ ($\vec{k}$ is the incident pion momentum and $\vec{k}'$ is the scattered pion momentum). $\sigma^0(\theta)$ is the unpolarized differential cross section, and iT_{11}, T_{20}, and T_{22} are the vector and tensor analyzing powers. From Eq. (4) it follows that

$$\frac{\sigma^+-\sigma^-}{\sigma^++\sigma^-}=\frac{\sqrt{2}\tilde{t}_{10}\langle iT_{11}\rangle}{1-\frac{1}{2}\tilde{t}_{20}\langle T_{20}\rangle-\sqrt{3/2}\tilde{t}_{20}\langle T_{22}\rangle}\ . \tag{5}$$

Typical values of the target vector polarization were 0.20; consequently, the tensor polarization $\tilde{t}_{20}$ as calculated from Eq. (3) is small ($\sim3\%$). Therefore, even if T_{20} and T_{22} assumed their maximum possible values over the entire angular range covered in this experiment, the tensor contributions to Eq. (5) are negligible. Dropping these terms, we obtain

$$\frac{\sigma^+-\sigma^-}{\sigma^++\sigma^-}=\sqrt{2}\tilde{t}_{10}\langle iT_{11}\rangle\ . \tag{6}$$

The relation between spherical and Cartesian vector target polarizations is $\tilde{t}_{10}=\sqrt{3/2}P$, and thus

$$iT_{11}=\frac{1}{\sqrt{3}}\frac{\sigma^+-\sigma^-}{P^-\sigma^++P^+\sigma^-}\ . \tag{7}$$

The uncertainty in iT_{11} is obtained from

$$\Delta iT_{11}=\frac{\{[P^++P^-]^2[(\sigma^-\cdot\Delta\sigma^+)^2+(\sigma^+\cdot\Delta\sigma^-)^2]+[\sigma^+-\sigma^-]^2[(\sigma^-\cdot\Delta P^+)^2+(\sigma^+\cdot\Delta P^-)^2]\}^{1/2}}{\sqrt{3}[P^-\sigma^++P^+\sigma^-]^2}\ . \tag{8}$$

In this expression, the $\Delta\sigma^+$ and $\Delta\sigma^-$ contain the statistical uncertainties in the measurements of the relative cross sections, and $\Delta P^{\pm}$ contains the relative uncertainty in determining the target polarization P. The various contributions to these uncertainties are further discussed in the following.

B. Polarized deuteron target

The polarized deuteron target evolved considerably during the course of the experiments which led to this publication. However, it was basically the same instrument used previously at SIN in experiments requiring a polarized proton target, a first version of which is described in Ref. 15. Characteristics of the polarized deuteron target which were unchanged for the various experiments include the following: The 2.5 T magnetic field was produced by a superconducting split coil magnet which supplied a vertical field homogeneous to one part in 10^4 over the volume of the target cell. The temperature of (typically) 0.5 K at the target cell was obtained with a ^{3}He refrigerator system. The target material consisted of a porphyrexide saturated mixture of 95% perdeuterated butanol (98% deuterated) and 5% deuterium oxide contained in a thin walled target cell with dimensions $5\times18\times18$ mm^3. In the initial parts of the experiment the target material was subdivided in 2 mm diameter spheres obtained by freezing drops of the butanol mixture in liquid nitrogen. Under these conditions only $\sim$60% of the cell volume was actually filled with polarizable material. In subsequent runs the butanol was frozen directly in the target cell, which resulted in a solid slab of frozen butanol stuck to the 0.08 mm brass walls of the target cell, which were in thermal contact with a ^{3}He reservoir located above the target cell. This new configuration eliminated background reactions from the ^{3}He coolant and the 1 mm Teflon target cell walls that were previously used. The target cell was usually positioned at 45 deg relative to the incident beam. The angle and location of the target cell relative to the magnet coils were verified for each experiment using x-ray techniques.

Dynamic polarization of the target was produced by irradiating the butanol with microwaves of approximately 70.1 GHz (for positive polarization) and 70.5 GHz (for negative polarization). The microwaves were supplied by mechanically coupling one of two independent microwave oscillators (one for each polarity) to a common waveguide into the target cell. In this technique, then, the target magnetic field remains constant during the entire experiment, and the different target polarizations are obtained strictly through the selection of a given microwave frequency. This eliminates all possible errors in the experiment which could arise from changes in the trajectories of the particles due to a change in the target magnetic field. The target superconducting magnet, equipped with a superconducting switch, was operated in persistent mode. The decay of the magnetic field was never allowed to exceed more than 2 G.

The deuteron polarization was determined by measuring the absorptive part of the nuclear magnetic resonance (NMR) signals detected by a constant current Q meter with a resonant tuned circuit. The output of an oscillator, swept in 32 msec between 16.1 and 16.5 MHz, was fed into the resonant circuit, and the voltage across the coil which was positioned in the median plane of the butanol target cell was amplified by a factor of 30 and rectified before being sent to a digital signal averager. The enhanced NMR signals were measured and recorded on magnetic tape every 5 min during the experiments. The area of the NMR signals is proportional to the relative polarization of the target. Underneath the NMR signal is a nonlinear background which is determined by the characteristics of the resonant circuit and by environmental noise pickup. At regular intervals during each experiment (typically once every two days) calibration measurements of the NMR signal baseline were obtained by decreasing the target magnetic field by 2.5%, which shifts the NMR signal outside of the frequency sweep range. By subtracting these baselines from enhanced NMR signals taken at nearly the same time, it was possible to obtain virtually background-free NMR signals. Analysis of these background subtracted signals indicated that the target polarization was stable to within 3% (relative) over a time period of several weeks. As a further check, the weighted average of the enhanced NMR signals accumulated every 5 min for each run (1—2 h) was also analyzed by fitting a polynomial function to the observed background and integrating the NMR signal above this background. The variation of the deuteron polarization as determined in the above manner for a typical run is shown in Fig. 1. This procedure should partially eliminate instabilities, drifts, etc., inherent in the measuring hardware but at the same time be more susceptible to errors in fitting the baseline. It was found that the polarizations was stable to within 5% (relative) over a period of several weeks. Among the factors contributing to this stability were the following two points: At least 15 min (about three times the polarization buildup time) was allowed for the polarization to reach its final value after a change of target polarity, and the frequency and power output of the microwave sources was continuously monitored.

The technique used to measure the absolute magnitude P of the target polarization was the same for all runs. The integrated area of the dynamically enhanced NMR

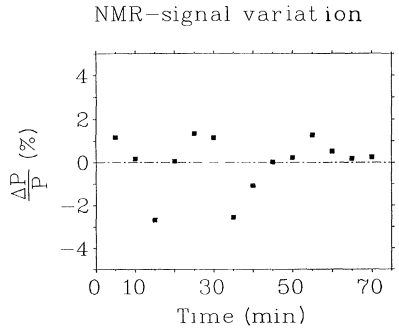

FIG. 1. The relative variation of the deuteron polarization is plotted as a function of time in minutes, for a typical run of positive polarization which lasted 1.5 h.

signal $A(D)$ was compared to that of the natural signal $A(N)$ as follows:

$$P=P(N)\frac{A(D)}{A(N)} .$$

Here, $P(N)$ is the absolute value of the deuteron polarization at thermal equilibrium (TE), which is given by

$$P(N)=\frac{4\tanh\left[\frac{\mu B}{2kT}\right]}{3+\tanh^2\left[\frac{\mu B}{2kT}\right]} , \tag{9}$$

where μ is the deuteron magnetic moment, k Boltzmann's constant, B the magnetic field, and T the temperature. This method of absolute calibration relies critically on the linearity of the NMR system, which was thoroughly verified over the relevant dynamic range, and on the ability to obtain an accurate measurement of the tiny TE NMR signal. Furthermore, an accurate measurement of the temperature is essential, and was performed by measuring the vapor pressure of the ^{3}He. In order to obtain $A(N)$, measurements of the TE signal were made at regular intervals, usually every week when the experiment was running. After turning off the magnetic field of the target to disorient the spin system, the field was again raised to 2.5 T and the TE polarization allowed to build up (without microwaves) for 8 to 12 h, which corresponded to roughly twenty times the deuteron relaxation time. Typical spectra obtained for both the natural and dynamic nuclear magnetic resonance (NMR) signals are shown in Fig. 2. The standard deviation of the resulting integrated NMR TE signal strengths was typically 10—15 % (relative), over an entire 4—5 week experiment. This was the dominant uncertainty in the experiment; however, it affects only the overall scale of the results, not the shape of the angular distributions. Typical values of the TE polarization were 0.11%, and 20% for the dynamically enhanced polarization.

During the course of the experiment the NMR signal detection was improved in several stages. The accurate measurement of the TE signal, which enters crucially in the absolute value quoted for iT_{11}, presented considerable difficulties. This is due not only to intrinsic reasons like the small magnetic moment of the deuteron and the large width of the NMR signal, but also to the electrically noisy environment in an accelerator laboratory and requirements imposed on the target configuration by the experiment. These requirements consist of the following: First, the target thickness must be kept small in order to either obtain good energy resolution for the scattered pions, or to allow recoil deuterons to escape the target. Second, as little material as possible (other than butanol) should be viewed by the projectiles and ejectiles; in other words the coolant, the NMR coil, the target cell walls, and the heat and vacuum shields had to be kept at an absolute minimum thickness.

With the above constraints in minds, the development of the NMR signal detection proceeded in steps. Initially a flat, wirewound spiral coil was positioned in the median plane of a copper cell with 0.08 mm thick walls. Two

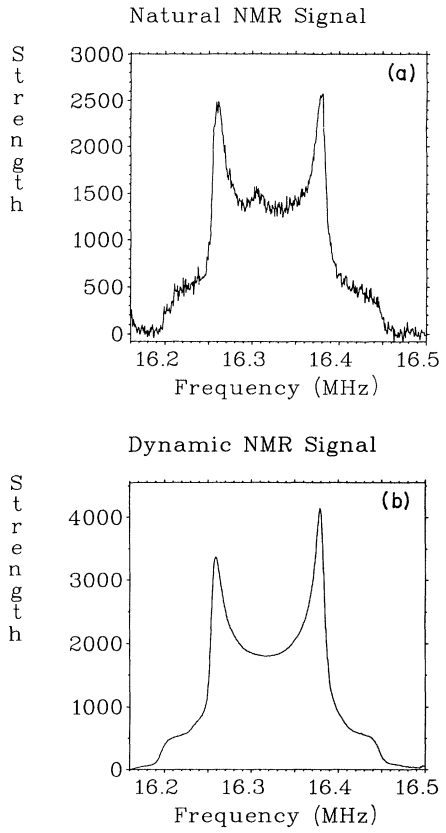

FIG. 2. (a) The thermal equilibrium deuteron magnetic resonance signal strength is shown as a function of the NMR frequency. (b) Same as for (a), only for the dynamically enhanced NMR signal.

layers of frozen butanol spheres filled the gaps between the walls of the target cell and the coil. The coil was connected through an 0.8 m long 50 Ω coaxial cable to a Varicap (a remotely variable capacitor) located outside the ^{3}He refrigerator, to build a series resonant circuit. Following this was a high frequency amplifier chain with an input impedence of 50 Ω. This system performed rather poorly, and therefore the copper cell was replaced by one of Teflon with 1 mm thick walls, to improve the Q value of the system. This change markedly improved the NMR signal strength and the signal-to-noise ratio, but considerably worsened the background in the πd elastic spectra. Most of the backward hemisphere measurements of iT_{11} described in the following were obtained under these conditions. Ultimately, a solution was found which reduced the background from the (Teflon) target cell and at the same time increased the NMR signal. Two separated coils were etched on the sides of a copper-clad 0.2 mm thick glass fiber reinforced Teflon plate, and connected in series to obtain the desired high inductance and mechanical stability. This coil was connected to a Varicap located roughly 5 cm above the target cell (inside the ^{3}He refrigerator), eliminating the long coaxial cable between the elements of the parallel resonant circuit. Following the Varicap (on the same circuit board) was a field-effect transistor (FET) amplifier to provide impedence matching

to the amplifier chain located outside the ^{3}He refrigerator. The same circuit has been used before only at temperatures down to 1.5 K (see Ref. 16). The target cell consisted of 0.08 mm thick brass. Larger NMR signals, better signal-to-noise ratios, and improved stability were achieved in this new configuration than with the previous arrangement employing the Teflon target cell and no low temperature electronics.

C. Forward hemisphere experimental arrangement

Data in the angular range corresponding to 30°—100° in the center of mass (c.m.) system were measured using the SUSI pion spectrometer and $\pi M1$ beamline at the Swiss Institute for Nuclear Research (see Fig. 3). As this facility has been described in detail in previous publications,[12] only those details pertinent to this experiment will be mentioned here. The $\pi M1$ channel is an achromatic system. It employs an electrostatic separator which delivers a pion beam of high purity at the target location. The beam size on target is approximately 1×1 cm^2 if a multiwire chamber is employed for the determination of the pion momentum at the intermediate focus. If this chamber is replaced by a 1 mm thick scintillation counter hodoscope for increased detection efficiency at higher pion fluxes, multiple scattering increases the beam size on target to roughly 2×2 cm^2. This is only slightly larger than the polarized target cell. In order to ensure that all of the counted beam particles hit the target, two thin scintillators were used upstream of the target, S1 and S2. The dimensions of S1 are 5 mm thick and 35×75 mm^2 in area. The beam defining counter $S2$ was 1 mm thick, 10×20 mm^2 in area, and located just upstream of the target vessel. The incident rate of positive pions, typically a few times 10^6 π^+/sec, allows one to count the incident beam directly. The incident beam was defined by the coincidence requirement BEAM=rf*$S1$*$\overline{S1}$*$S2$, where rf was the cyclotron radio frequency timing signal, and $\overline{S1}$ was a veto signal from an upper level pulse height threshold set on $S1$ to eliminate the few protons which got through the separator.

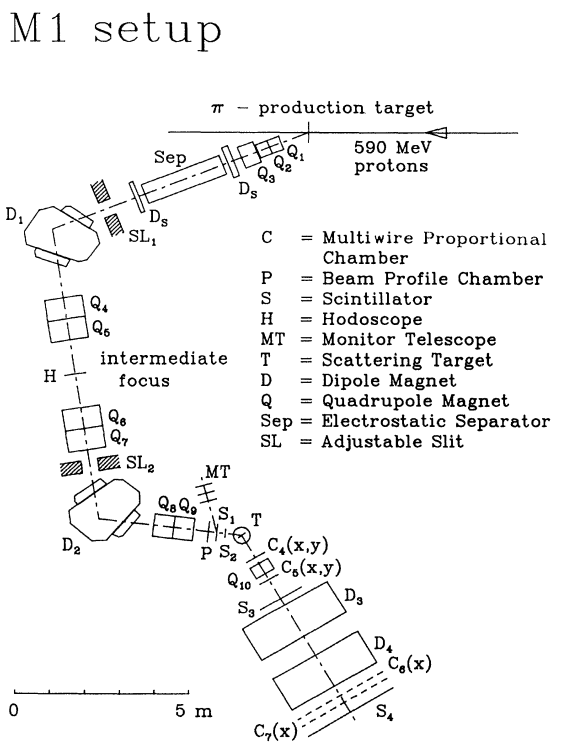

FIG. 3. Experimental arrangement used for the measurements on the $\pi M1$ channel and SUSI spectrometer.

The beam momentum at the target center was determined from the magnetic field in the second bending magnet, the measured effective field length for this magnet, the calculated optical properties of the transport system, and the calculated energy loss of the pions in the material upstream of the target center. The absolute momentum scale should be accurate to $\pm0.3\%$.[54]

Scattered pions then passed through a pair of wire chambers surrounding a quadrupole magnet and a thin (1 mm) scintillator $S3$ before being deflected 135 deg in the spectrometer, after which they impinged on a focal plane detection system consisting of a pair of 2 m wire chambers and another scintillator $S4$. An event was defined by the coincidence requirement BEAM*$S3$*$S4$. A three element monitor telescope MT used as a check on the incident beam normalization viewed pions scattered from $S2$. The incident beam profile was continuously visually monitored by use of a beam profile chamber PC located in between $S1$ and $S2$. The incident beam was centered on the polarized target by maximizing the πd event rate as a function of the horizontal and vertical location of $S2$. The angular acceptance of the spectrometer was 10 deg.

A typical pion energy loss spectrum is shown in Fig. 4(a). The carbon and oxygen ground states were always well separated from the πd elastic peak. However, at some angles small contributions from the inelastic states of these nuclei appeared in the region of πd elastic scattering. Therefore background measurements on normal (nondeuterated) butanol were taken at each angle [Fig. 4(b)]. In this way the background due to the other (unpolarized) nuclei present in the polarized target was explicitly measured for later subtraction. A typical background subtracted spectrum is shown in Fig. 4(c). Naturally, a subtracted spectrum of this kind reflects a negative peak from the hydrogen in the background target which was not present in the foreground target. However, this peak was always well separated from the deuterium. The energy resolution was typically 2.5 MeV. After background subtraction, the pion energy loss spectra exhibited the following features: To the left (higher energy) side of the πd elastic peak the background was very small. To the right side a pedestal from deuteron breakup could be observed starting 2.2 MeV from the centroid of the elastic peak. Finally, to the extreme right, the dip due to hydrogen subtraction appears. At some angles the background contributions from carbon and from the NMR pickup coil were also investigated. It was found that replacement of the deuterated butanol with normal butanol provided the cleanest background subtraction.

From these spectra, the relative cross sections for πd

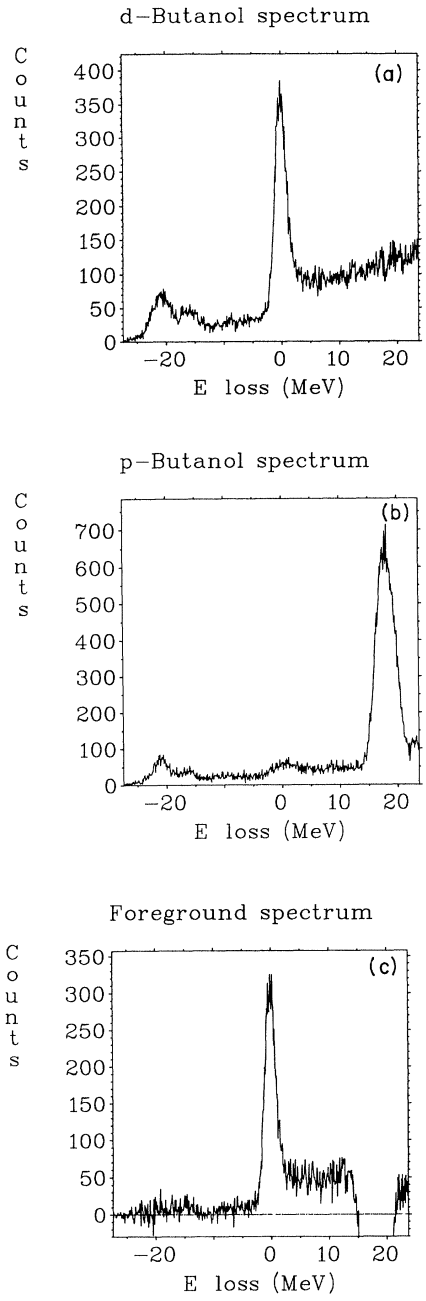

FIG. 4. (a) A sample spectrum of the pion energy loss is shown, as measured with the polarized deuteron target. This spectrum was taken at an incident pion energy of 134 MeV, and at a center of mass angle of 90 deg. The peak centered at zero energy loss corresponds to πd elastic scattering, the events near -20 MeV E loss arise from carbon and oxygen contaminants. (b) A background spectrum measured with a target consisting of normal butanol (C_4H_9OH) taken under the same conditions as described in (a). The large peak on the right arises from pion elastic scattering on hydrogen. (c) Spectrum obtained by subtracting the spectrum shown in (b) from that in (a). It represents the events which arise solely from the deuterons in the polarized target, minus those which arise from the hydrogen in the background target. The pedestal to the right of the πd elastic peak comes from events in which the deuteron dissociates. The background from the carbon and oxygen has been eliminated.

elastic scattering needed to compute the vector analyzing power as in Eq. (7) were obtained from the expression

$$\sigma^{\pm}=\frac{\text{yield}^{\pm}}{\text{BEAM}\cdot\epsilon_{\text{hodo}}\cdot\epsilon_{\text{chmbr}}\cdot\epsilon_{\text{comp}}}\ , \tag{10}$$

where BEAM, defined above, is the number of incident pions, and the efficiencies are those for the hodoscope, the wire chambers, and the computer. Typical values of these efficiencies were 0.90, 0.55, and 0.75, respectively. The yield represents the number of πd elastic scattering events, and was obtained in one of several different ways, described in the following.

Uncertainties in the measurements of the relative cross sections can arise from the following sources: the statistical error in the yield (foreground minus background), poor determinations of the background used to extract the yield, or drifts in the electronics. Many of these uncertainties can be reduced by a systematic treatment of the data in which the target polarization is switched several times. Data for a given angle were always measured in a sequence of at least eight runs (data taking periods) of different polarities, i.e., $+--++--+$, followed by background measurements. Each run of a given polarity lasted between 1 and 2 h. One approach used to analyze the data, therefore, was to add all the runs of a given polarization together, fit the πd elastic peaks, and use the resulting relative cross sections with their counterparts of opposite polarization in Eq. (7). This was done both with and without explicit subtraction of the true background measured separately from normal butanol. In all cases, however, the yield used to extract a relative cross section was determined by assuming the πd elastic peak had a Gaussian shape and sat on top of a linear background which was also fit and removed. The alternative approach was to determine the eight relative cross sections separately, and construct a four by four matrix of iT_{11} values calculated from each pair of relative cross sections of opposite polarization. The diagonal of this matrix represents the time ordered sequence of iT_{11} measurements, and was used to determine the final, weighted average of iT_{11} at a given angle. The off diagonal elements were used as checks for possible systematic errors. This procedure (again done both with and without explicit subtraction of the normal butanol background) made it possible to easily verify the consistency of the individual measurements, which together yielded the value of iT_{11} for a single given angle. As a further check on the consistency of the data reduction, each of the methods quoted above was performed on nine different histograms of the pion energy loss, each of which had different software gates applied to it or different binning. In this way it was possible to identify and eliminate possible errors from poor fitting or incorrect software cuts such as might arise from drifts in the electronics of the system. Therefore, the uncertainties in the relative cross sections used in Eq. (8) to calculate the uncertainty in iT_{11} contained only the statistical errors of the πd elastic peak area and the background underneath it. Consistency of all 36 analyses of iT_{11} was demanded for each angle measured in this experiment.

The use of the pion spectrometer was necessary to separate the πd elastic events from elastic events on other nuclei at forward angles, where recoil deuterons do not escape from the target. At larger angles where this recoil information was available, however, the relatively small (15 msr) solid angle of the spectrometer becomes a considerable drawback as the differential cross section for πd elastic scattering falls several orders of magnitude between 20 and 90 deg, as well as falling rapidly with increasing bombarding energy. Consequently, the measurements of iT_{11} with the pion spectrometer were limited to these forward angles in this part of the experiment.

D. Backward hemisphere setup

In order to overcome the limitations imposed by the small solid angle of the pion spectrometer, in particular where the πd elastic differential cross section is small, a different experimental arrangement for the backward hemisphere measurements was devised (see Fig. 5). In this new arrangement, a sixfold array of pion scintillation counter telescopes was employed in coincidence with an array of six associated recoil deuteron scintillators and proton veto counters. A given pion telescope was composed of two scintillators in coincidence which viewed the target region only. The first element was 5×16 cm^2 in area, 3 mm thick, and 0.5 m from the target [$\pi1(i)$, $i=A,F$]. The second element of the pion arm [$\pi2(i)$, $i=A,F$] was 10×35 cm^2 in area, 5 mm thick, and at 1 m from the polarized target it defined the solid angle of 30 msr per counter, and the angular acceptance of 5 deg per counter. The $\pi2$ counters were viewed at each end by a photomultiplier tube in order to obtain optimum timing resolution. For each pion arm at a given angle, there was a corresponding recoil deuteron counter [$D1(i)$, $i=A,F$] whose angle was adjusted to correspond to recoil deuterons from πd elastic scattering. These counters (10×40 cm^2 in area, 5 mm thick) were 1.3 m from the target, and were also viewed at each end by a phototube. Following each deuteron counter was an absorber whose thickness was adjusted to stop recoil deuterons from πd elastic scattering at that angle. Following the absorbers were veto counters [$D2(i)$, $i=A,F$].

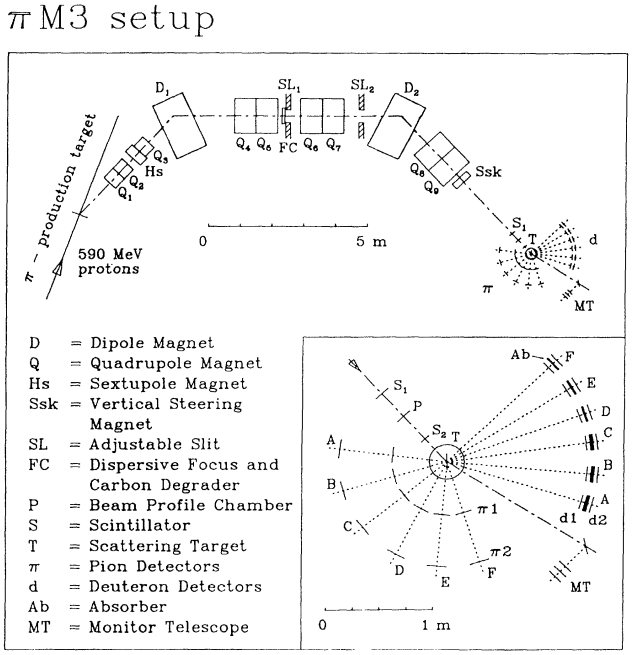

FIG. 5. The experimental arrangement for the measurements performed on the $\pi M3$ channel. The detector array is displayed with a larger scale in the inset.

The pulse height information from each counter was recorded on magnetic tape, as well as the timing information from the $\pi2$ and $D1$ counters. The apparatus was arranged to measure six angles simultaneously. Due to the larger solid angle, the reduced pion decay losses from the shorter pion flight path, the absence of inefficiencies in multiwire chambers, and the sixfold detector multiplicity, an overall factor of more than 20 was gained in the efficiency of data acquisition with this experimental arrangement in comparison to the pion spectrometer, for those angles where the two techniques overlap.

This arrangement was set up in the $\pi M3$ beam channel at SIN. The beam definition, in terms of two in-beam scintillators $S1$ and $S2$, was the same as on SUSI. Scintillator $S2$ defined the target location. On this beamline, however, proton contamination in the incident beam was reduced with differential degrading in a 5 mm carbon absorber located in between the two channel dipole bending magnets. The event definition consisted of the coincidence

$$\text{BEAM}\cdot\pi1(i)\cdot\pi2(i)\cdot D1(i)\cdot\overline{D2(i)}\ .$$

As on the SUSI experiment, the kinematics were calculated using a ray tracing program which utilized a map of the target magnetic field, and incorporated energy loss effects in the target cell and the surrounding thermal shields. For example, pions of 256 MeV were deflected 17 deg as they passed through the target magnet.

The beam momentum at the target center, including the effect of energy loss in the carbon absorber, was determined from a field chart of the first channel dipole magnet, and checked with particle range measurements.[55] The mean beam momentum is known to a precision of $\pm0.4\%$.

The signature of a πd elastic scattering event was obtained from the difference in the $D1$ and the $\pi2$ (stop) signals. The start signal for the CAMAC time-to-digital converters (TDC's) was the event coincidence, with the rf signal determining the timing. By using the difference of the two stop signals, the jitter in the time of arrival of the start signal was eliminated. Previous tests had indicated that this quantity produced the best separation of πd elastic events from πp quasielastic and πd$\rightarrow$2p reactions. A typical spectrum showing this separation is shown in Fig. 6. The πp and πd$\rightarrow$2p contributions have been reduced by use of the veto counter as well as by software gates on the $\pi1$, $\pi2$, and $D1$ pulse heights.

A major concern with this experimental arrangement was whether the πd quasielastic events from carbon would be peaked in the TOF distribution underneath the πd elastic events. This was checked for several angles and energies in a separate test run using carbon, CD_2, and ^{3}He tar-

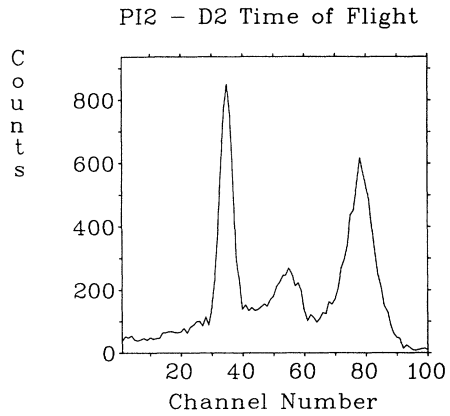

FIG. 6. Typical spectrum of the difference in time of flight between pions and their associated recoil deuterons. This spectrum was accumulated at a bombarding energy of 256 MeV, at a center of mass angle of 140 deg. The peak on the left corresponds to πd elastic scattering events, the peak in the middle to πp quasielastic events, and the peak on the right to πd$\rightarrow$2p events. The contributions from the latter two reactions have been suppressed by means of the veto counters.

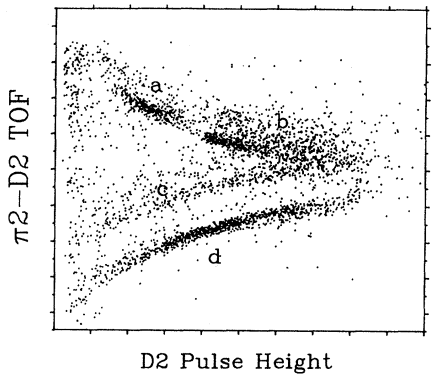

FIG. 7. Two-dimensional density plot of the difference in time of flight between pions and their associated recoil deuterons (vertical axis) and pulse height in the deuteron scintillator (horizontal axis). The conditions were 256 MeV incident pions, detected at a center of mass angle of 78 deg. The labels *a*, *b*, *c*, and *d* refer to events from πd$\rightarrow$2p, πp quasielastic, πd$\rightarrow\pi$pn, and πd elastic, respectively.

gets. The background was found to be flat and small. Since the background in the TOF histograms underneath the πd elastic peak was fit and subtracted from the peak itself (as already described in the spectrometer experiment), it was possible to account for this (unpolarized) background in the analysis.

The instrumental (timing) resolution was better than 0.5 nsec (corresponding to an energy resolution of 2.7 MeV for 50 MeV deuterons), although the kinematic broadening of the πd elastic reaction worsened this by a factor of 2—3. This resolution was adequate for clean separation of πd elastic events from other reactions whenever the deuterons had enough kinetic energy to pass through the $D1$ counter (passing mode). For the smallest scattering angles, however, the deuterons stopped in the $D1$ counter (stopping mode), and the one-dimensional TOF spectrum no longer showed a clean separation of deuterons and protons. For these cases, on the other hand, two-dimensional spectra of the $D1$ pulse height versus the $D1-\pi2$ TOF displayed a well-separated band of deuterons from protons (see Fig. 7). Therefore a polygon was drawn around the deuteron band in this two-dimensional spectrum to separate πd elastic events from the background. This technique was checked by test measurements with CD_2 and carbon targets, as well as by independent measurements for several angles with the SUSI pion spectrometer.

As a final test of the system, measurements of the πd differential cross section were performed using a CD_2 target. The results obtained both with and without explicit subtraction of spectra from a carbon background target agreed to within 5% of the published values of Gabathuler *et al.*[17] At small scattering angles, some of the recoil deuterons with very low kinetic energy stopped in the target. A Monte Carlo correction for this target thickness effect was able to account for the difference in cross section over the entire angular range measured in the subsequent polarization experiments. While this test demonstrated that the system could be used to measure absolute differential cross sections, it should be stressed that no such measurements were necessary in order to obtain iT_{11}. Only the relative cross sections for positive and negative target polarization need to be measured at a given angle to obtain iT_{11}. In fact, the absolute differential cross sections measured with the polarized target were used as a check for possible systematic errors.

The measurement algorithm and the analysis of these data proceeded in a similar way as on SUSI. The formula used for the relative cross section was the same, except that no hodoscope or wire chambers were used, and that the "area" was obtained differently depending on whether or not the recoil deuterons were in passing or stopping mode. For angles in which the recoil deuterons were in passing mode, a variety of histograms with different gating conditions were fit. As with the SUSI data, all fits were done by subtracting a linear, fitted background to the data surrounding the πd elastic peak, which was assumed to be Gaussian. As the previously quoted tests with CD_2 and carbon targets had indicated that the background underneath the πd elastic peak was small and flat, no separate runs with a background target were taken in this experimental arrangement, and just the fitted background was subtracted. The different software gates applied included loose and tight cuts on the $D1$, $\pi1$, and $\pi2$ pulse heights, as well as a loose gate around the $\pi2$ TDC signal to eliminate randoms. As with the SUSI data, a measurement of iT_{11} at a given angle consisted of a sequence of at least eight runs, analyzed with the matrix technique already described. For angles in which the recoil deuterons were in stopping mode, the number of events inside the polygon drawn around the πd band in the two-dimensional display of $D1$ pulse height vs TOF was used, for both individual and summed runs. As the test runs had indicated that only very little background appeared in this region, the uncertainty in the yield for

TABLE I. The measured values of iT_{11} in πd elastic scattering are tabulated versus pion bombarding energy and c.m. angle. The values of iT_{11} and the uncertainties in iT_{11} are in percent. The notations (a—g) indicate the experimental condition for a given angle, where a refers to SUSI data from Ref. 7 (renormalized by $\frac{2}{3}$), b refers to SUSI data from Ref. 8 (renormalized by $\frac{2}{3}$), c refers to TOF data (passing mode, see text) measured in 1982, d refers to TOF data (stopping mode, see text) measured in 1982, e refers to TOF data (passing mode) measured in 1983, f refers to TOF data (stopping mode) measured in 1983, and g refers to SUSI data measured in 1983.

T_π	θ	iT_{11}	ΔiT_{11}	Notation	T_π	θ	iT_{11}	ΔiT_{11}	Notation
117.0	114.5	17.6	6.4	f		152.2	3.9	2.0	d
	121.4	22.8	4.5	f		161.0	6.6	1.9	d
	126.3	10.3	4.3	f					
	130.6	5.1	3.3	f	142.0	70.0	28.1	6.7	a
	135.4	3.6	3.6	f		90.0	32.2	6.7	a
	139.6	7.3	3.0	f		110.0	29.5	6.7	a
	144.3	6.7	3.2	f		125.0	14.1	6.0	a
	148.5	2.5	2.7	f		140.0	12.1	5.4	a
	153.1	−1.2	3.1	f					
	158.4	0.0	2.0	f	151.0	94.0	29.5	5.6	f
						104.0	20.3	3.1	f
125.0	108.0	27.5	8.1	f		106.8	27.6	3.0	f
	110.5	19.1	6.1	f		111.3	22.2	2.7	f
	115.4	17.2	2.5	f		116.5	22.8	2.5	f
	120.0	10.0	3.6	f		120.9	16.3	2.4	f
	124.8	12.6	1.7	f		125.9	15.5	2.4	f
	129.3	8.2	3.0	f		135.2	12.9	2.3	f
	133.9	7.9	1.7	f		144.2	9.6	2.2	f
	138.4	4.8	2.6	f		151.1	6.3	2.3	f
	140.6	8.9	2.2	f		153.1	15.0	2.2	f
	143.1	9.5	1.9	f		159.8	5.7	2.9	f
	147.2	8.9	1.8	f					
	151.9	4.0	1.9	f	180.0	37.7	2.8	3.5	g
	157.6	4.4	1.7	f		49.1	7.2	4.4	g
	158.4	2.2	2.2	f		71.5	16.8	3.9	g
	165.0	0.5	3.3	f		83.2	33.5	3.3	f
						90.2	18.6	4.8	g
134.0	48.4	2.8	3.3	g		90.9	34.3	3.2	f
	70.5	10.9	3.9	g		96.1	35.1	3.0	f
	89.3	12.3	5.1	g		101.1	30.4	2.9	f
	104.0	14.5	5.3	f		106.1	26.0	2.7	f
	109.0	17.3	3.8	f		111.0	29.7	6.0	e
	110.0	9.8	5.5	g		120.8	18.6	5.9	e
	113.7	20.0	2.9	f		130.2	16.9	5.0	e
	118.6	18.6	2.7	f		139.5	21.6	4.2	e
	123.1	15.5	2.4	f		148.5	10.8	4.4	e
	128.0	15.0	2.5	f		157.4	5.0	4.2	e
	132.4	13.7	2.1	f					
	137.1	10.0	2.2	f	219.0	40.6	3.3	3.4	g
	141.5	10.0	2.1	f		55.0	5.8	4.6	b
	146.1	9.4	2.1	f		70.0	20.8	4.4	b
	150.4	7.8	2.0	f		77.9	13.1	3.3	f
	155.0	6.7	2.1	f		85.0	26.1	5.4	b
						93.6	31.5	3.6	f
140.0	72.5	18.6	4.7	g		100.0	26.9	5.2	b
	98.0	34.1	7.5	f		111.3	30.1	5.4	e
	105.3	19.2	3.7	f		120.9	22.8	5.1	e
	115.0	16.7	2.8	f		130.0	12.2	6.6	b
	119.0	16.4	3.5	d		141.8	16.8	5.6	e
	122.1	18.0	2.8	f					
	131.4	8.4	2.5	f	238.0	40.0	−1.6	3.2	g
	134.0	14.0	2.6	d		54.0	0.8	4.0	g
	140.5	9.4	2.3	f		66.0	2.3	3.4	f
	143.0	11.9	2.1	d		74.2	6.1	2.1	f

TABLE I. (*Continued*).

T_π	θ	iT_{11}	ΔiT_{11}	Notation	T_π	θ	iT_{11}	ΔiT_{11}	Notation
	82.1	19.9	2.5	f		70.0	−9.3	3.5	c
	90.0	18.5	3.2	f		75.0	−9.8	4.4	b
	97.7	34.5	6.1	e		81.0	−4.6	5.2	c
	107.8	31.6	3.9	e		91.0	14.7	8.1	c
	108.1	30.2	6.0	e		102.0	27.4	5.7	c
	117.9	22.8	5.7	e		112.0	32.9	6.0	c
	127.3	23.7	5.0	e		121.0	26.6	4.9	c
	136.5	13.2	4.7	e		131.0	8.7	5.1	c
	145.5	16.5	4.7	e		131.0	9.3	6.0	c
	154.2	1.4	5.0	e		140.0	6.0	4.2	c
						149.0	0.1	5.7	c
256.0	32.7	3.9	5.2	g		157.0	−4.2	5.9	c
	44.5	1.5	5.3	g					
	55.0	15.4	4.7	a	294.0	45.0	−10.7	4.7	b
	55.0	13.9	3.6	b		46.0	−0.7	7.2	g
	56.1	−0.4	3.7	g		55.0	−11.6	4.0	b
	56.1	−3.2	4.9	g		57.7	−8.2	5.8	g
	62.2	1.9	3.2	f		65.0	−19.4	5.5	b
	67.4	−1.6	6.8	g		69.0	−10.1	2.4	d
	68.0	0.2	7.1	d		75.0	−14.3	4.7	b
	70.0	−2.7	5.4	a		80.0	−11.2	3.9	d
	70.0	−3.4	4.5	b		85.0	7.4	4.8	b
	76.1	4.7	2.1	f		91.0	29.9	13.5	c
	78.0	9.4	3.2	d		100.0	35.2	7.2	b
	84.1	13.9	2.8	f		101.0	34.0	6.6	c
	85.0	14.1	6.7	a		111.0	25.9	10.6	c
	89.0	14.8	3.2	d		121.0	23.3	6.0	c
	90.0	31.5	3.7	c		130.0	4.3	6.5	b
	100.0	30.2	5.4	a		130.0	10.6	5.2	c
	100.0	35.6	7.6	b		141.0	−1.0	4.1	c
	100.0	29.1	3.5	c		148.0	−0.8	5.0	c
	107.2	26.2	6.0	e		157.0	6.0	3.5	c
	110.0	15.5	5.5	c					
	114.5	26.1	6.2	e	325.0	54.2	−11.5	2.3	f
	115.0	20.7	8.0	a		60.0	−11.9	3.2	d
	120.0	25.0	3.9	c		66.0	−16.7	2.7	d
	124.0	23.8	5.9	c		74.0	−14.0	2.8	d
	129.0	20.0	5.2	c		77.0	−20.5	3.4	d
	130.0	−10.7	8.0	a		79.3	−23.2	5.4	e
	133.0	20.2	4.9	c		88.0	5.9	7.0	d
	140.0	9.2	4.0	c		90.2	−9.6	6.4	e
	145.0	10.7	5.4	a		100.8	33.0	8.5	c
	149.0	8.3	4.8	c		110.8	13.9	6.4	e
	160.0	5.1	5.3	c		120.2	16.5	9.4	e
						125.0	7.5	5.0	c
275.0	40.8	−2.0	3.7	g		136.0	−4.7	7.2	c
	55.0	−2.3	4.2	b		145.0	−1.3	4.7	c
	65.0	−5.3	4.0	b		154.0	−1.4	4.3	c

these cases was taken to be purely statistical. Otherwise, the analysis for stopping mode runs proceeded exactly the same as for the passing mode runs.

III. RESULTS

The results of all the new and existing iT_{11} measurements are tabulated in Table I. The measurement technique is indicated for each point. The previously published SUSI data are also presented in this table (renormalized by $\frac{2}{3}$). The main feature of the data can be described as the following: As the incident pion energy is raised, the smooth, bell-shaped angular distribution of iT_{11}, develops a dip at forward angles (near 70 deg) which becomes more and more pronounced at energies above 256 MeV. The maximum of about 30% in the angular distribution of iT_{11} occurs near 100 deg, where the differential cross section has a minimum. The agreement between these results and previous measurements of iT_{11} is good,

with the exception of data at two angles at 256 MeV (55° and 130° c.m., see Table I). Due to improvements in the polarized target, the scattering background could be reduced considerably, and from explicit background measurements its subtraction is more reliable now compared to that employed in the previously published results.[7,8] In that light, the uncertainty due to background subtraction at 55 deg has apparently been underestimated in the previous data. At 130°, the TOF system involved much higher counting rates and therefore shorter runs, which are less susceptible to systematic uncertainties. The new data cover the region from 117 to 325 MeV in 12 steps. At each energy an average of 14 angles have been studied. This completeness allows for the first time the study of the behavior of iT_{11} with sufficient statistics, angles, and energies to compare reliably with the theoretical predictions.

The experimental results between 134 and 325 MeV are shown in Fig. 8, along with the results of fits employing Legendre polynomials to guide the eye. Measurements at the same angle have been averaged for clarity in the figure. It was found that up to six terms were required in the fit in order to obtain a satisfactory description of the data over the entire range of angles and energies studied. The results of these fits have been used to generate a three-dimensional plot of iT_{11} vs angle and bombarding energy (Fig. 9) which more clearly shows the behavior of iT_{11} in the regime covered by these experiments. This figure underscores the smooth transition in incident energy between a bell-shaped angular distribution and one in which a minimum asserts itself at forward angles.

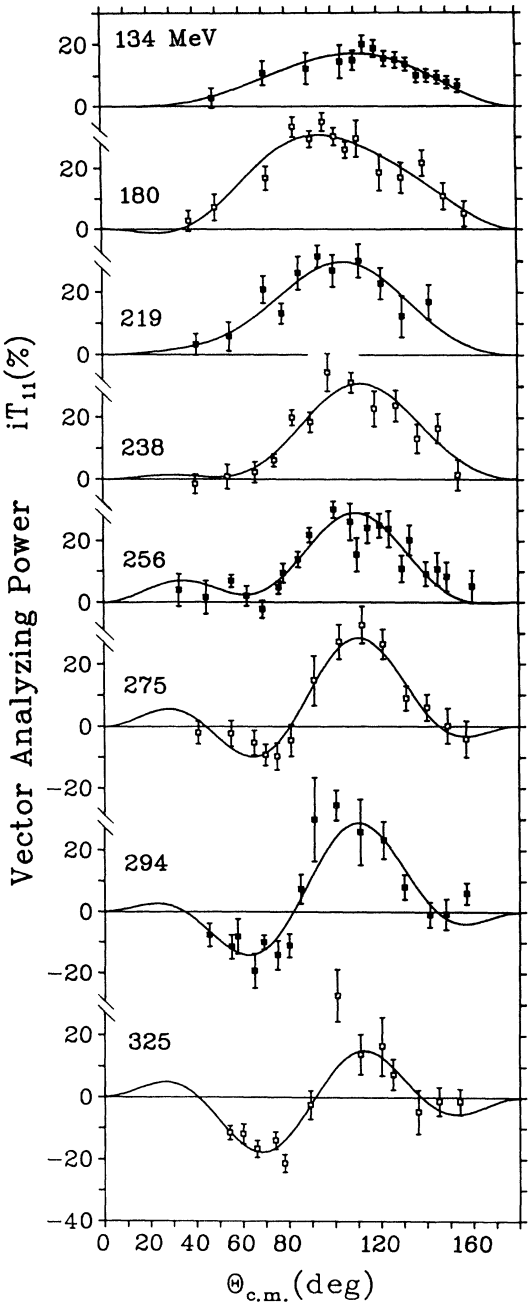

FIG. 8. The values of the vector analyzing power iT_{11} measured in the πd elastic scattering reaction are shown versus center of mass angle for most of the energies measured in this experiment. Some results from previous measurements have been included, and data at some angles have been averaged. Data from some of the angles and energies included in Table I have not been shown for clarity. The curves (to guide the eye) were generated from fits to the data using a six term Legendre polynomial.

IV. THEORETICAL PREDICTIONS

In this section the experimental results are compared with various theoretical calculations. First we shall discuss theories that are based on "conventional dynamics," i.e., meson exchange mechanisms. Then we shall show how effects due to dibaryon resonances or quark degrees of freedom may change these predictions. In general, it should be emphasized that the considerable experimental effort in the πd system has in past years been matched by extensive theoretical work. In fact, on the theoretical side, the elastic πd channel is the best studied and most well understood pion nucleus system to date. It is for this reason that any discrepancies between theory and experiment are significant.

To begin with, the most ambitious theoretical effort, Faddeev-type three body calculations, have been steadily refined to a high degree of sophistication over a period of ten years. Initially, these calculations were used to study the N-d system. In the application to πd scattering, relativistic kinematics for the pion were introduced while the nucleons were treated nonrelativistically. Then Rinat and Thomas[18] developed a "fully" relativistic approach in order to extend the calculations from low energies to the region of the (3,3) resonance. For the two body input into the Faddeev calculations, it was found that details of the nucleon-nucleon interaction (the $^3S_1$-$^3D_1$ NN channels) have only little influence on the observables. On the other hand, the input of the πN partial waves is very important. In the beginning only the P_{33} channel was retained. The addition of small S and P waves had little effect on the cross section at 140 MeV, but dramatic changes in the angular distribution of iT_{11}. Already the first measurements of iT_{11} at 140 MeV (Ref. 7) demonstrated the importance of the small S and P partial waves. Finally, it was realized that pion absorption and the NN→NN

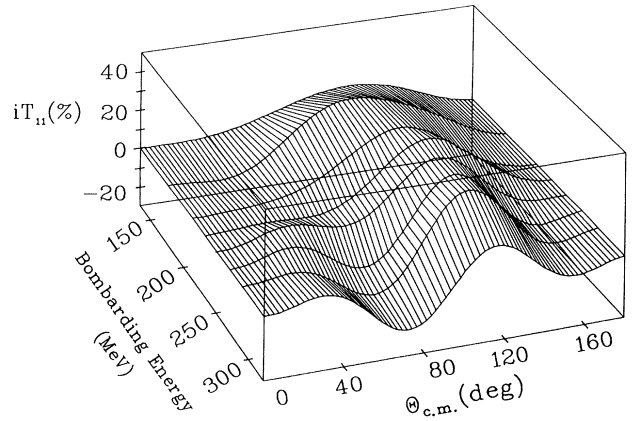

FIG. 9. A three-dimensional representation of the existing iT_{11} data for the πd elastic scattering reaction. The contours were generated from the Legendre polynomial fits shown in Fig. 8. This figure shows the general trend of the data with respect to angle and energy, namely the smooth onset of a dip at forward angles with increasing bombarding energy.

channel should be included in a description of πd scattering. The coupled πNN→NN system has been extensively studied within the context of three body scattering theories. As a consequence, a set of coupled integral equations has to be solved involving the amplitudes $T(\pi d \rightarrow \pi d)$, $T(\pi d \rightarrow NN)$, $T(NN \rightarrow NN)$, and $T(NN \rightarrow \pi d)$, where the NN channel stands for the NN* channel as well. For a review of πd Faddeev calculations, see Ref. 19.

A particular problem is the treatment of the P_{11} partial wave in the πN subsystem. This partial wave, which accounts for true pion absorption, is split into a pole part and a nonpole part $t(P_{11}) = t(P) + t(\mathrm{NP})$, where $t(P)$ is the direct nucleon-pole contribution, and t(NP) is the remaining background. Although the P_{11} is a small partial wave ($\delta_{11} < 2°$ for $T_\pi < 150$ MeV), it is an important quantity in the three body calculations since the two large contributions $t(P)$ and t(NP) enter the Faddeev calculations separately and in different places [not simply as the sum of $t(P) + t(\mathrm{NP})$].

The development of the Faddeev-type three body calculations has been carried out mainly by three groups. While these groups basically use the same formalism, they differ in some important practical aspects, especially in the way the P_{11} partial wave is split. The main features of each approach are briefly described in the following paragraphs.

In the Flinders calculations,[20–24] relativistic kinematics are used only for the pion. Rho and omega exchange are neglected, which implies almost no spin-orbit interaction. The P_{11} amplitude is parametrized with a two term separable potential and fit to the P_{11} phase shifts.[23] No constraint on the scattering volume or the πNN on-shell coupling constant was imposed; the πNN vertex function is energy independent in this model. Several parametrizations are presented which fit the P_{11} phases equally well for T_π up to 250 MeV, but deviate rapidly from experiment for higher energies. Although each parametrization leads to a similar prediction of the πd differential cross section, quite different predictions of the vector analyzing power are generated depending on which fit is used. The parametrization which is preferred by these workers is the one which gives the best description of the πd→2p total cross section. The vector analyzing power iT_{11} is also best described by this (arbitrary) choice of parametrization.

The Lyon group[25–31] treats the baryons and the pion relativistically. Heavy meson exchange is not included. The P_{11} amplitude is represented by a two parameter fit to the scattering volume and the phase shifts.[30] The fit is constrained such that the (energy dependent) πNN vertex function has the observed NN coupling constant as residue at the nucleon pole. The general energy dependence of the πNN vertex function is discussed in Refs. 30 and 32. This constraint was not applied in the Flinders calculations,[23] which use an energy independent vertex function. According to Mizutani *et al.*,[31] the Lyon approach conserves exact two and three body unitarity, in contrast to the Flinders parametrization. Test calculations of the Lyon group indicate that breaking three body unitarity can change the predictions of the πd differential cross section (e.g., at 256 MeV) by up to a factor of 3 at angles larger than 90 deg.[31]

The predictions of Rinat *et al.*[33–37] fall into two categories. The first set of calculations are fully relativistic, satisfy two and three body unitarity, include rho exchange, and include pion absorption and emission. However, the nonpole part of the P_{11} was omitted. In a more recent publication,[37] this omission was rectified. Rinat points out that even in the distorted wave impulse approximation, the $T(\pi d \rightarrow NN)$ amplitude is proportional to the final state NN interaction.[37] For low partial waves the latter is influenced by rho and omega exchange, which is neglected by the other groups.

When comparing the predictions from the three groups, one finds good agreement with the measured differential cross sections[17] up to 180 MeV. At higher energies (256 MeV) systematic discrepancies with the cross section data exist in the backward hemisphere, with the Rinat group doing somewhat better than Lyon, and the Flinders group doing better still. Regarding the vector polarization (see Fig. 10) there is fair agreement among the various predictions and with the data up to 180 MeV. Above this energy the results from the Lyon group and from the Rinat group (Refs. 33–36) agree with each other. They predict a bell-shaped angular distribution of iT_{11} which has a maximum near 70 deg for all energies calculated (up to 294 MeV). The predictions of Ref. 37 are similar, except the maximum has moved further out in angle to near 100 deg, in agreement with the experimental results. Remarkable, however, is the fact that none of these predictions can account for the minimum in the experimental data which develops at 70 deg with increasing bombarding energy. The results of the Flinders calculations are similar to those of Ref. 37 in that they correctly predict the location of the experimentally observed maximum in iT_{11} near 100 deg. They differ from all other predictions in the sense that they predict a slight dip in iT_{11} at 256 MeV near 70 deg. The forward angle dip at higher energies can be qualitatively accounted for in the Flinders calcula-

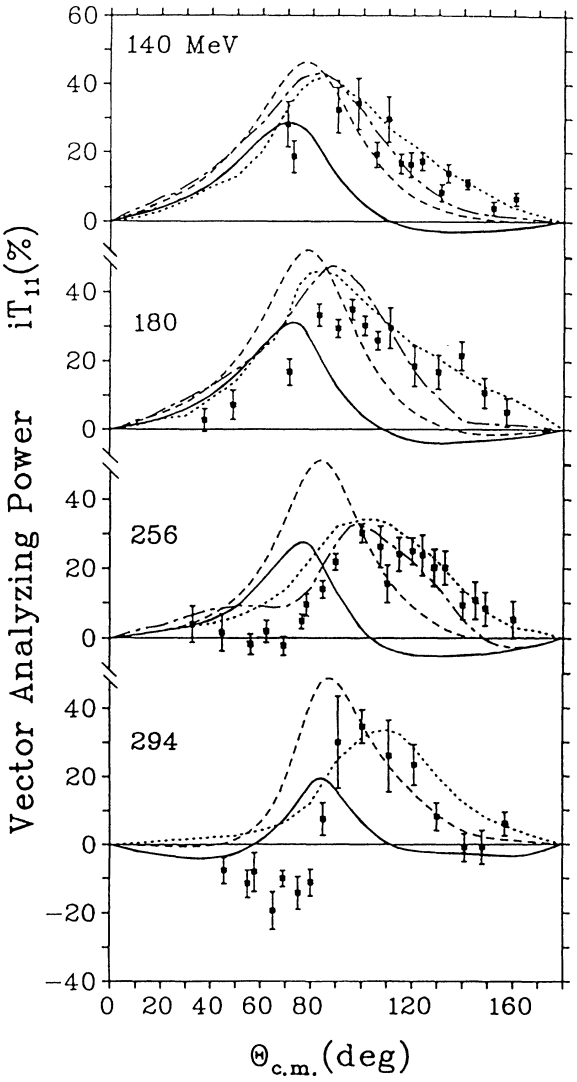

FIG. 10. The iT_{11} data at four different incident energies are compared to various theoretical predictions: impulse approximation (solid curve), Lyon (dashed curve), Refs. 37 and 48 (dotted curve), and Flinders (dash-dot curve). No predictions above 256 MeV are available from the Flinders group. These energies are deemed crucial since the main feature of the measured energy dependence of iT_{11} is the development of a forward angle dip which is prominent above 256 MeV. None of the available predictions based on conventional dynamics can describe this feature of the data.

tions,[38] although to date these predictions remain unpublished. At present, it seems plausible to speculate that this feature of the Flinders calculations arises from their treatment of the P_{11}. As mentioned above, however, this is the weakest point of their approach. Rinat *et al.*[37] consider their failure to implement the renormalization of the nucleon propagator and πNN vertex a serious omission. Whether or not the predicted forward angle dip in the Flinders calculations survives a more refined treatment of the P_{11} remains to be seen. If in the future such calculations from this group are able to correctly describe the angular dependence of iT_{11} at higher energies (e.g., 294 MeV), it will be important to pin down the cause for this improvement within the framework of the other calculations.

At this point it may be illustrative to compare at forward angles the various Faddeev predictions with the results of an impulse approximation (IA) calculation (see Fig. 10), which includes all S and P πN partial waves in the two body input.[39] In the IA calculation of iT_{11} the gradual development of a minimum is observed at forward angles and the magnitude of the predicted iT_{11} values is reasonable, but the angle at which the maximum occurs is shifted too far forward, as is the case with the Lyon predictions and the early predictions[33–36] of the Rinat group. Test calculations showed that interference effects with the P_{11} phase are important for the vector polarizations, as expected.

Recently Betz and Lee[40] proposed a model of the interactions between pions, nucleons, and delta isobars and applied it to the πd system. Great efforts went into a good description of the NN channel. Since only the resonant P_{33} amplitude was kept in the application to πd elastic scattering, the results for the vector polarization are not relevant to the present discussion. The model so determined gives a satisfactory description of pion absorption by deuterons and of the elastic πd scattering cross sections, but fails to reproduce iT_{11} and t_{20}. The model is presently being refined.

For completeness, other πd calculations should be mentioned, for example, the D^* model by Händel *et al.*[41] The underlying N-Δ interaction in this model has recently been refined.[42] While the total and differential cross sections have been reproduced, the polarization observables are not properly described.

Based on a description of the physical delta-isobar as a dynamic πN system, a realistic force model for the two nucleon system including delta and pion degrees of freedom has been constructed by Popping, Sauer, and Zhang Xi-Zhen.[43] The πd partial wave amplitudes are derived from the NΔ T matrix and the π-N-Δ vertex. In spite of the limitations of this model, the differential cross sections for πd elastic scattering are well reproduced between 140 and 292 MeV. There is qualitative agreement with the iT_{11} data only up to 217 MeV.

Summarizing, one can state that none of the published calculations based on conventional dynamics have been able to reproduce the entire set of iT_{11} data. It will be interesting to see if further refinements, in particular with regard to the treatment of the P_{11} πN partial wave amplitude (intimately connected with a satisfactory treatment of pion absorption), will be able to correctly describe all observables (including NN amplitudes) measured so far.

In the meantime one may raise the question of whether the systematic discrepancies between measured and calculated vector analyzing power at higher energies can be explained by some "nonconventional reaction dynamics." Shortly after the discovery of the anomalous behavior in the energy dependence of the spin dependent total NN cross sections,[2] and its interpretation in terms of dibaryon resonances, Kubodera *et al.*[44] and Kanai *et al.*[45] mixed the isospin one dibaryon resonances $^1D_2$, $^3F_3$, and $^1G_4$ into Faddeev partial waves and Glauber amplitudes,

respectively, and predicted the effects of dibaryon resonances on the differential cross section and the vector and tensor polarizations. More recently, the same approach has been used to cite evidence for dibaryon resonances in πd differential cross section measurements at much higher (300–1000 MeV) energies.[4–6] A continuation of these theoretical studies led to detailed predictions of the effects of dibaryon resonances on all πd observables.[46] Earlier measurements of iT_{11} suggested that such effects were needed in order to obtain a satisfactory description of the then sparse data set. However, the lack of a comprehensive set of iT_{11} measurements prevented a definitive comparison. With the large scope of iT_{11} data available now, this study has been repeated. For the time being, the conflicting measurements of t_{20} have been neglected. The calculations were performed using the computer code of Ref. 47. First, the importance of the $^1D_2$, $^3F_3$, and $^1G_4$ resonances was investigated separately for each resonance, keeping the mass M and the total width Γ fixed, and varying the partial width $\Gamma(\pi d)$, the orbital mixing α, and the relative phase γ to fit the iT_{11} data. In a second step the search was extended to two dibaryon resonances to establish their relative contributions. The conclusions are similar to those drawn from the previous effort. A good fit to the iT_{11} data can be made; however, the description of the differential cross section is poor, particularly at large angles where the Faddeev "background" amplitudes are too high and are not considered to be accurate. The optimal fit requires a combination of the $^1D_2$ and $^1G_4$ dibaryon resonances. In a further study, similar results were obtained when fits were made to iT_{11} and the forward angle differential cross sections simultaneously. The results are shown in Fig. 11 and Table II. Clearly, these results do not present definite evidence for the existence of dibaryon resonances as long as the failure of the conventional models is not firmly established. In particular, the strong contribution from the $^1D_2$ (2200 MeV) is probably a reflection of inadequacies in the treatment of the leading N-Δ dynamics. Furthermore, it is not possible to uniquely establish the internal structure of such resonances in this kind of analysis.

Recently in an alternate approach, Rinat speculated about the possibility that the πd vector analyzing power data may reveal quark substructure of baryons for unexpectedly low q^2.[48] The πd observables were calculated in a cloudy bag model description for an intermediate delta isobar. In these predictions, the only adjustable parameter was the bag radius, which was fitted to the P_{33} πN transition amplitude. Differential and total cross sections were well described in this exploratory study, while the observed angular variation in iT_{11} at higher energies was qualitatively described without involving the coupling of dibaryon resonances to πd (see Fig. 12). The conclusion of these studies is that the πd vector polarization data reveal quark substructure of the standard qqq configuration for single baryons.

As for the NN→NN and the NN→πd channels, a phase shift analysis for the πd elastic channel may reveal resonance effects in a model independent way. In particular, starting from Faddeev amplitudes that describe reasonably well the total and differential cross sections

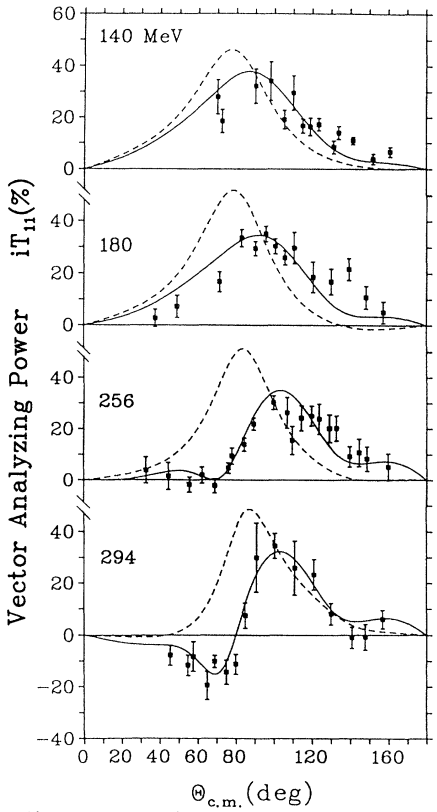

FIG. 11. The same experimental data discussed in Fig. 10 are compared to predictions employing "nonconventional dynamics." The standard Lyon predictions (dashed curve) are shown for reference. The admixture of $^1D_2$ and $^1G_4$ dibaryon resonances to these (Lyon) predictions results in the fit depicted by the solid curve.

and searching only on specific amplitudes, a phase shift analysis may produce some clue as to which partial waves are responsible for the characteristic behavior of the iT_{11} angular and energy dependence. The first phase shift analysis of elastic πd scattering was performed by Arvieux and Rinat,[49] and by Arvieux.[50] After the first t_{20} data appeared in the literature, Hiroshige *et al.*[51] investigated the consistency of iT_{11} and t_{20} data in a phase shift analysis. All three analyses were based on a limited data set for iT_{11} and t_{20}. The consistency of the iT_{11} and t_{20} data is further discussed in Ref. 52. In spite of the much expanded iT_{11} data base made available in this publication, however, the limited number of measured observ-

TABLE II. Dibaryon resonance parameters defined as in Ref. 47, where M is the invariant mass, Γ the total width, $\Gamma(\pi d)$ the partial width to the pion deuteron channel, α the angular momentum coupling angle, and γ the phase with respect to the background.

	$^1D_2$	$^1G_4$
M (MeV)	2200.0	2480.0
Γ (MeV)	85.0	150.0
Γ (πd) (MeV)	25.0	9.0
α (deg)	19.7	90.0
γ (deg)	26.3	3.2

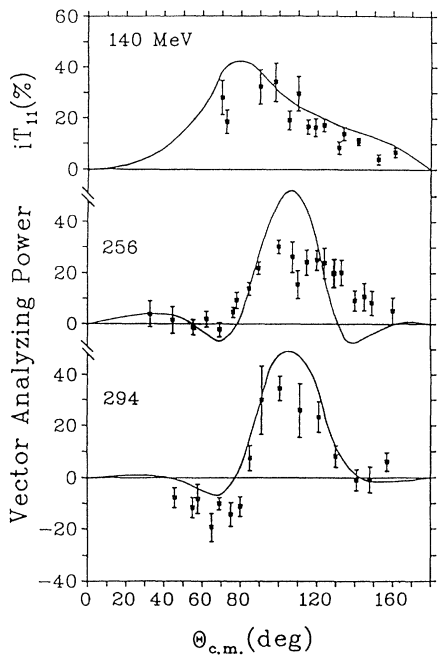

FIG. 12. Same experimental data as shown in Fig. 11. The curve depicts the predictions of Rinat which employ a cloudy bag model description for an intermediate delta isobar.

ables will not uniquely determine the phase shifts.[53] Conclusions based upon such an analysis, therefore, are not relevant to the present discussion.

V. SUMMARY AND CONCLUSIONS

Angular distributions of the vector analyzing power iT_{11} for 12 incident energies between 117 and 325 MeV have been presented. The data show the onset of a dip near 70 deg which becomes more pronounced as the bombarding energy is raised above 256 MeV. Faddeev calculations using a realistic prescription for the P_{11} pion-nucleon amplitude fail to describe this feature of the data. By adding Breit-Wigner (dibaryon resonance) amplitudes to these Faddeev amplitudes, the data can be well described. Faddeev calculations performed using a different prescription for the P_{11} amplitude are reportedly able to qualitatively reproduce the vector polarization data without the need for inclusion of dibaryon resonances. Finally, exploratory calculations employing a description of an intermediate delta based upon the cloudy bag model are in qualitative agreement with the vector polarization data at all energies measured, again without the necessity of including dibaryon resonances.

In conclusion, the comprehensive set of iT_{11} data presented here put highly sophisticated conventional theories to a stringent test. At present, it cannot be ruled out that a more refined treatment of some ingredients of the calculation, in particular pion absorption (through the P_{11} partial wave), may eventually reconcile the existing discrepancies with the experimental data. If, however, the failure of the conventional models to describe all the iT_{11} data persists, an approach including some new degree of freedom (e.g., dibaryon resonances) may be necessary.

ACKNOWLEDGMENTS

We wish to express our thanks to Dr. M. P. Locher, Prof. A. S. Rinat, and Dr. M. E. Sainio for many invaluable theoretical discussions during the course of this work. Also, we would like to thank Prof. R. R. Johnson, Dr. R. Frosch, and Ms. G. Schmidtlein for help in parts of the experimental set up. This work would have been impossible without the generous help and considerable skills of the staff of SIN. This work was supported in part by the Bundesministerium für Forschung und Technologie of the Federal Republic of Germany.

[1]A. Aerts, P. Mulders, and J. de Swart, Phys. Rev. D 21, 2653 (1980).
[2]A. Yokosawa, Phys. Rep. 64, 47 (1980).
[3]J. J. Aubert *et al.*, CERN Report No. CERN-EP/83-14, 1983; R. L. Jaffe, Phys. Rev. Lett. 50, 228 (1983); A. Bodek *et al.*, *ibid.* 50, 1431 (1983).
[4]R. C. Minehart *et al.*, Phys. Rev. Lett. 46, 1185 (1981).
[5]M. Akemoto *et al.*, Phys. Rev. Lett. 50, 400 (1983).
[6]M. Akemoto *et al.*, Phys. Rev. Lett. 51, 1838 (1983).
[7]J. Bolger *et al.*, Phys. Rev. Lett. 46, 167 (1981).
[8]J. Bolger *et al.*, Phys. Rev. Lett. 48, 1667 (1982).
[9]R. J. Holt *et al.*, Phys. Rev. Lett. 43, 1229 (1979); 47, 472 (1981); E. Ungricht *et al.*, *ibid.* 52, 333 (1984).
[10]J. Ulbricht *et al.*, Phys. Rev. Lett. 48, 311 (1982); W. Gruebler *et al.*, *ibid.* 49, 444 (1982); in *High Energy Spin Physics—1982,* Proceedings of the Fifth High Energy Spin Symposium, AIP Conf. Proc. No. 95, edited by G. M. Bunce (AIP, New York, 1983), p. 235.
[11]S. E. Turpin *et al.*, Nucl. Phys (to be published).
[12]R. Balsiger *et al.*, Nucl. Instrum. Methods 157, 247 (1978); J. P. Albanese *et al.*, *ibid.* 158, 363 (1979).
[13]G. R. Smith *et al.*, Phys. Rev. C 25, 3228 (1982).
[14]*Proceedings of the Third International Symposium on Polarization Phenomena in Nuclear Reactions, Madison, 1970,* edited by H. H. Barschall and W. Haeberli (University of Wisconsin, Madison, 1971).
[15]C. Amsler, ETH Zurich, Dissertation No. 5621, 1975.
[16]H. R. Wampach and N. S. Sullivan, Rev. Sci. Instrum. 49, 1622 (1978).
[17]K. Gabathuler *et al.*, Nucl. Phys. A350, 253 (1980).
[18]A. S. Rinat and A. W. Thomas, Nucl. Phys. A282, 365 (1977).
[19]A. W. Thomas and R. H. Landau, Phys. Rep 58, 121 (1980).
[20]I. R. Afnan and A. W. Thomas, Phys. Rev. C 10, 109 (1974).
[21]I. R. Afnan and B. Blankleider, Phys. Lett. 93B, 367 (1980).
[22]I. R. Afnan and B. Blankleider, Phys. Rev. C 22, 1638 (1980).
[23]B. Blankleider and I. R. Afnan, Phys. Rev. C 24, 1572 (1981).
[24]I. R. Afnan and A. T. Stelbovic, Phys. Rev. C 23, 1384 (1981).
[25]N. Giraud, G. H. Lamot, and C. Fayard, Phys. Rev. Lett. 40, 438 (1978).

[26]N. Giraud, Y. Avishai, C. Fayard, and G. H. Lamot, Phys. Lett. 77B, 141 (1978); Phys. Rev. C 19, 465 (1979).
[27]Y. Avishai and T. Mizutani, Nucl. Phys. A326, 352 (1979); 338, 377 (1980); 352, 399 (1981); Phys. Rev. C 27, 312 (1983).
[28]C. Fayard, G. H. Lamot, and T. Mizutani, Phys. Rev. Lett. 45, 524 (1980).
[29]N. Giraud, C. Fayard, and G. H. Lamot, Phys. Rev. C 21, 1959 (1980).
[30]T. Mizutani, C. Fayard, G. H. Lamot, and R. S. Nahabetian, Phys. Rev. C 24, 2633 (1981).
[31]T. Mizutani, C. Fayard, G. H. Lamot, and R. S. Nahabetian, Phys. Lett. 107B, 177 (1981).
[32]W. T. Nutt and C. M. Shakin, Phys. Rev. C 16, 1107 (1977).
[33]A. S. Rinat, Nucl. Phys. A287, 399 (1977).
[34]A. W. Thomas and A. S. Rinat, Phys. Rev. C 20, 216 (1979).
[35]A. S. Rinat, E. Hammel, Y. Starkand, and A. W. Thomas, Phys. Lett. 80B, 166 (1979); Nucl. Phys. A329, 285 (1979).
[36]A. S. Rinat, Y. Starkand, and E. Hammel, Nucl. Phys. A364, 486 (1981).
[37]A. S. Rinat and Y. Starkand, Nucl. Phys. A397, 381 (1983).
[38]I. R. Afnan, private communication; B. Blankleider, private communication.
[39]M. P. Locher, private communication.
[40]M. Betz and T.-S. H. Lee, Phys. Rev. C 23, 375 (1981); T.-S. H. Lee, Phys. Rev. Lett. 50, 1571 (1983).
[41]R. Händel, M. Dillig, and M. G. Huber, Phys. Lett. 73B, 4 (1978).
[42]H. G. Hopf, Ph.D. thesis, University of Erlangen, 1983 (unpublished).
[43]H. Popping, P. U. Sauer, and Zhang Xi-Zhen, Nucl. Phys. (to be published).
[44]K. Kubodera and M. P. Locher, Phys. Lett. 87B, 169 (1979).
[45]K. Kanai, A. Minaka, A. Nakamura, and H. Sumiyoshi, Prog. Theor. Phys. 62, 153 (1979).
[46]W. Grein and M. P. Locher, J. Phys. G 7, 1355 (1981).
[47]M. P. Locher and M. E. Sainio, Phys. Lett. 121B, 227 (1983).
[48]A. S. Rinat, Phys. Lett. 126B, 151 (1983).
[49]J. Arvieux and A. S. Rinat, Nucl. Phys. A350, 205 (1980).
[50]J. Arvieux, Phys. Lett. 103B, 99 (1981).
[51]N. Hiroshige, W. Watari, and M. Yonezawa, Prog. Theor. Phys. 68, 327 (1982).
[52]E. L. Mathie *et al.*, Phys. Rev. C 28, 2558 (1983).
[53]M. Meyer, Ph.D. thesis, University of Erlangen, 1983 (unpublished).
[54]E. Pedroni *et al.*, Nucl. Phys. A300, 321 (1978).
[55]J. C. Alder *et al.*, Phys. Rev. D 27, 1040 (1983).